Advanced Optical Materials / Volume 11, Issue 16 / 2300111

Research Article | Full Access

Second Harmonic Generation in Exfoliated Few-Layer ReS_2

Ying Song, Yuwei Shan, Weiming Wang, Kainan Chang, Ze Zheng, Zhiming Shi, Dabing Li, Jin Luo Cheng

First published: 19 May 2023
https://doi-org.fgul.idm.oclc.org/10.1002/adom.202300111

Abstract

The second harmonic generation (SHG) is systematically investigated in mechanically exfoliated, few-layer ReS_2 samples. The stacking orders are identified as $(AA)_nA$ and $(AB_y)_nA$ for (2n+1)-layer samples and $(AA)_n$ and $(AB_y)_n$ for 2n-layer samples. The layer structure A stands for that of a monolayer, and the layer structure B_y is mirror to A followed by a one-tenth unit cell translation along the mirror axis, that is, the ***b***-axis of the crystal. Only the even-layer samples with $(AB_y)_n$ stacking order are SHG active. After carefully extracting the effective bulk susceptibility for SHG, it is found that the spectra are greatly enhanced as the fundamental photon energy matches exciton levels. The polarization dependence is strongly anisotropic, and each susceptibility component shows very different wavelength dependence. The results demonstrate that few-layer ReS_2, with its unique SHG, can be considered as an ideal platform for fundamental research in anisotropic nonlinear optics.

1 Introduction

ReS_2, a member of 2D transition metal dichalcogenides (TMD) family, has attracted considerable interest due to its anisotropic optical,[1-5] vibrational,[6, 7] electronic,[8] and ferroelectric properties.[9] These arise from its distorted 1T crystal structure, where the Re—Re bonds form chains of parallelograms due to the additional valence electrons of Re atoms, as shown in **Figure 1a**. The monolayer structure has the very low symmetry C_i point group,[10] with a spatial inversion center. Similar to other TMD materials, few-layer ReS_2 also exhibits interesting nonlinear optical response, including third harmonic generation (THG),[11] nonlinear optical absorption,[12] and second harmonic generation (SHG).[9, 13-15] ReS_2

exhibits an extremely strong third-order nonlinear susceptibility $|\chi^{(3)}|$, on the order of magnitude 10^{-18} m^2 V^{-2}. Zhou et al.[16] observed that the nonlinear optical absorption in thick ReS_2 samples strongly depends on the polarization angle and stacking order. The existence of inversion symmetry in monolayer ReS_2, in analogy to that in graphene, leads to vanishing SHG under the electric dipole approximation,[13] although small signals have been observed from the substrate effect at an excitation wavelength of 1045 nm.[14] For multilayer samples, Song et al.[13] detected extraordinary SHG signals in even-numbered layers and negligible signals from odd-numbered layers at an excitation wavelength of 1558 nm. However, Dhakal et al.[14] found remarkable SHG signals, varying with layer number continuously up to over 20 layers, regardless of the layer number parity. As long as a gate voltage was applied, SHG can be generated in few-layer ReS_2 with both layer number parities.[15] Further, with temperature increasing from room temperature to around 405 K, SHG in bilayer ReS_2 vanishes due to a crystal phase transition.[9]

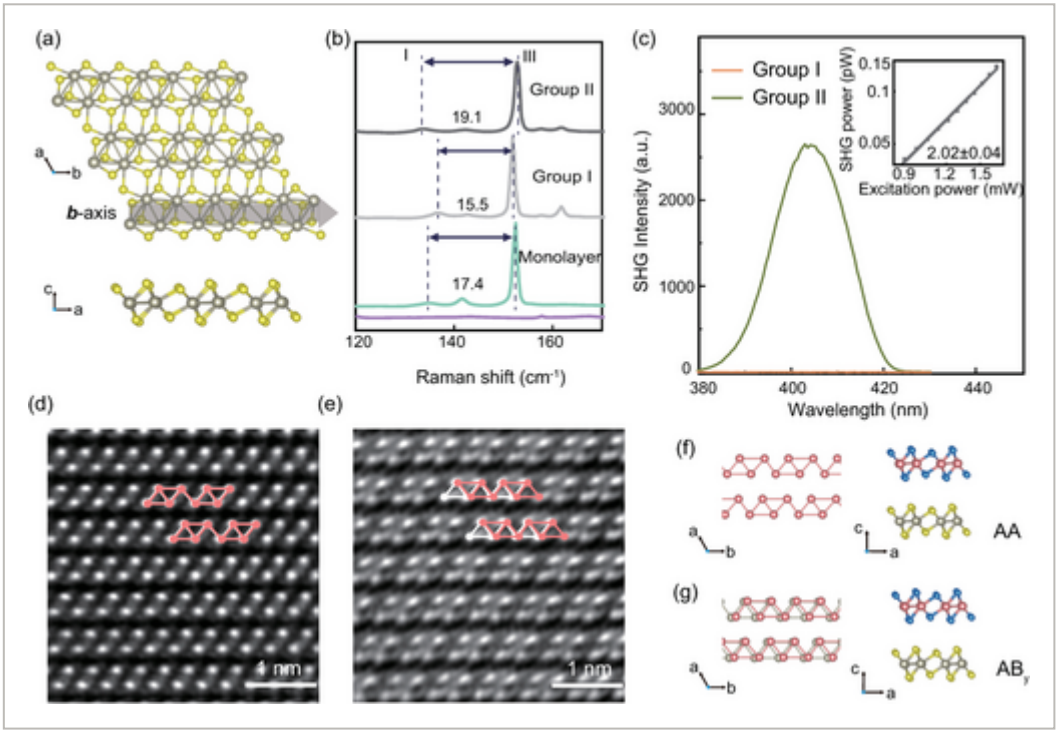

Figure 1

Open in figure viewer | PowerPoint

a) Schematic diagram of a crystal structure for monolayer ReS_2: top view (upper) and side view (bottom). Gray (yellow) balls represent Re (S) atoms. The gray arrow indicates Re—Re bond chains, which are along the direction of the ***b***-axis. b) Raman spectra of bare substrate (violet line), monolayer ReS_2 (green line), and bilayer ReS_2 in group I (gray line) and group II (black line). The excitation polarization is parallel to the direction of the ***b***-axis. The numbers on the graph between the two dotted lines represent the differences between the modes III and I. c) SHG spectra from bilayer samples in group I and group II for fundamental excitation wavelength at 809 nm with average power of 0.85 mW. The angle between the excitation polarization and ***b***-axis of ReS_2 is fixed at 20°. The inset gives the power dependence of SHG intensity on a log-log scale, with a fitted slope 2.02 ± 0.04. STEM images of bilayer samples d) group I and e) group

II with proposed relative replacement between two layers. Schematic diagrams of crystal structures of f) AA and g) AB_Y stacking orders: top view (left) and side view (right).

It is surprising that reports in the literature indicate that all even-layer ReS_2 samples can generate SHG signals at room temperature. Taking bilayer ReS_2 as an example, a simple stacking of two inversion symmetric monolayer ReS_2, where the upper layer has only a relative displacement to the lower layer, cannot break the inversion symmetry to generate SHG, as is the case for AA/AB-stacked bilayer graphene[17] and bilayer CrI_3.[18] With respect to the SHG active bilayer samples, additional stacking operations, such as mirror symmetric operation[9, 19] or relative rotational operation[20] to form a Moiré pattern, should exist. The stacking structure of ReS_2 is usually experimentally characterized by Raman spectroscopy[16, 21, 22] and scanning transmission electron microscope (STEM) measurements,[22] interpreted with the assistance of density functional theory (DFT) calculations.[21-23] Polarization-dependent Raman spectroscopy implies that the relative rotation between layers by an angle of 60° or 120°[21] is unlikely, since mechanically exfoliated few-layer samples have a clearly defined ***b***-axis along orientation of Re–Re chains.[6] Meanwhile, whether or not a mirror operation plays a role in the appearance of SHG at room temperature has not yet been verified. Therefore, the understanding of the effect of stacking geometry on SHG is still incomplete, even for bilayer ReS_2.

Another interesting but not well investigated problem is how the excitonic effects affect the optical nonlinearity for strongly anisotropic materials. Due to the insufficient screening of Coulomb interaction, excitonic effects in 2D materials always play an important role in optical properties, and they can lead to a remarkable exciton resonance in the SHG spectra of some TMD materials.[24, 25] In ReS_2, the excitons are unique because the nearly degenerate levels lead to optical absorption with a strong polarization dependence.[10] Although it was claimed that the excitation photon energy can be used to control the SHG intensity,[15] direct experimental evidence for the excitonic effects has not been reported, and how its anisotropy affects SHG is unclear.

In this work, we find that SHG in even-layer ReS_2 can be both active and inactive, while odd-layer samples are all inactive. For SHG active samples, inversion symmetry is broken because adjacent layers are formed by stacking a second layer as a mirror image of a first layer, but with a translation along the mirror axis (the ***b***-axis). We further investigate the dependence of the effective SHG susceptibilities on the photon energy and the layer number. For fundamental photon energies between 0.74 and 1.55 eV, the SHG intensity can vary up to two orders of magnitude, and the SHG intensity dependence on the layer number can be completely opposite for different photon energies. These findings suggest that various methods are available for controlling the SHG signal from ReS_2 flakes, which can lead to flexible strategies for developing tunable photonics devices.

2 Discussion and Results

2.1 Stacking Orders of Few-Layer ReS_2

Few-layer ReS_2 samples were fabricated on polydimethylsiloxane (PDMS) substrates by mechanical exfoliation of bulk ReS_2 crystals. Raman spectroscopy at an excitation wavelength of 532 nm was used to characterize the layer number,[6] the crystal axis;[6] preliminary stacking classification[21, 22] was obtained from the wavenumber difference (Δ) between Raman modes III and I, as shown in Figure 1b. For monolayer ReS_2, Δ is 17 cm^{-1}; for multilayer ReS_2, the values of Δ are classified into two groups (I and II). For group I (II), Δ ≈ 15 cm^{-1} (19 cm^{-1}) for bilayer samples, and Δ decreases (increases) monotonically when increasing the layer number (see the detailed confirmation of layer number dependent Δ in Figure S2a,b, Supporting Information). Based on the report by Zhou et al.,[22] where the positions of Re atoms are further confirmed by STEM images, group I (II) is identified as AA (AB) stacking order, with different relative displacement. These two groups also show distinct optical absorption (Figure S4, Supporting Information).

We performed SHG measurements with these samples in a reflection geometry with normally incident light, provided by a linearly polarized femtosecond laser at 809 nm with an average pulse power of 0.85 mW, repetition rate of 80 MHz, and pulse width of 151 fs. The signal around 404.5 nm was collected. No signal was detected from the PDMS substrate (Figure S5a, Supporting Information). Remarkable SHG signals were observed from even-layer samples in group II, and negligible signals were detected for all others. As an example, Figure 1c shows the SHG spectra for bilayer samples in these two groups. The signal of group II is confirmed as SHG by the quadratic dependence on the pump power with a power index of 2.02 ± 0.04. The inactive SHG bilayer samples in group I is consistent with our analysis considering a simple displacement between the upper and lower layers as reported by Zhou et al.,[22] which does not break the inversion symmetry. The nonzero SHG signals from bilayer samples in group II force us to re-examine their stacking structures, which should go beyond the simple displacement claimed in previous literature.[22]

The stacking orders of group I and II are identified from the following three aspects. First, we identify the direction of the ***b***-axis by Raman spectra (Figures S2c and S3, Supporting Information) and exclude the possibility of relative rotation between two layers. For more details see in Part 1 in the Supporting Information. The polarization dependence of Raman mode V indicates the orientation of the Re—Re chains (***b***-axis), and our bilayer samples in both groups show the same polarization dependence as that of the monolayer ReS_2 (Figure S2c, Supporting Information). Therefore, any relative rotation between the two layers is unlikely. A possible way to break the inversion symmetry without changing the orientation of Re—Re chains is to introduce a mirror plane,[9] as discussed in the crystalline phase transition at high temperature.[9] The mirror planes are considered to be the *xy*, *yz*, or *zx* plane (the coordinate system is chosen to set the *y*-axis along the ReS_2' ***b***-axis and the *z*-axis perpendicular to the plane, see Figure S1, Supporting Information, for atomic structure diagram of different mirror plane), where the case of *xy* mirror plane gives consistent Re

atom in-plane coordinates with the STEM image reported by Tongay et al.[3] To clarify the crystal structure of each layer, we denote one reference monolayer as A, the other layer with relative displacement as B and with further mirror symmetry as B_i (i = z, x, y for the *xy, yz, zx* mirror planes, respectively). Second, to investigate the atomic structures of group I and group II we performed STEM images of the samples, where the positions of Re atoms are imaged, as shown in Figure 1d,e. Although the STEM images of groups I and II are different, the well-defined Re—Re chains (***b***-axis) are both clearly observed, suggesting no relative rotation between layers. Figure 1d shows an arrangement of Re atoms for the bilayers in group I, which is very similar to the published STEM image of monolayer ReS_2.[6] The bilayer samples in group II show a rather complicated pattern (Figure 1e), with periodic bright spots but indistinguishable positions of adjacent Re atoms. Among those three mirror operations mentioned above, the case of a *zx* mirror plane can generate the closest STEM patterns. Third, according to the SHG results the bilayer samples in group I are center inversion symmetric and those in group II are not, as shown in Figure 1f,g. Therefore, we identify samples in group I as having AA stacking order, where there is no displacement between adjacent layers, while those in group II have AB_y stacking order, which includes a mirror operation with respect to the *zx* plane and a displacement of about one-tenth of the unit cell along the ***b***-axis (see in Supporting Information).

Based on the results in bilayer ReS_2, we consider the stacking order and SHG for other few-layer ReS_2 samples. Group I and II also include samples with layer number between 3 and 6. SHG of all samples in group I vanish (Figure S5b, Supporting Information), which indicate the AA stacking order with inversion symmetry in all layer numbers. The situation for samples in group II is much complicated. **Figure** 2 shows the white light image (Figure 2a) and SHG signal microscopy image (Figure 2b–d) of a sample from group II, which ranges from bilayer to six-layer of ReS_2 continuously in one region. The SHG signals are generated by excitation with femtosecond pulses with average power of 0.3 mW at fundamental photon energies of 0.8, 0.97, and 1.54 eV, respectively. Regardless of the excitation photon energy, the SHG signals vanish for odd-layer samples, and they are observable for even-layer samples (Figure S6, Supporting Information), which suggests that inversion symmetry is maintained only in the odd-layer samples. In these samples, there exists an overlap region between different layers, which can be used to identify the stacking order: for the bilayer, the stacking order is AB_y, as discussed above; for the three-layer, the third layer should be inversion symmetric to the first layer, and gives the stacking order as AB_yA; for the five-layer, the fourth and fifth layers should be inversion symmetric to the second and first layers, respectively, and give the stacking order as AB_yAB_yA. Therefore, we determine the stacking order for group II as $(AB_y)_n$ for even-layer ReS_2 and $(AB_y)_nA$ for odd-layer ReS_2.

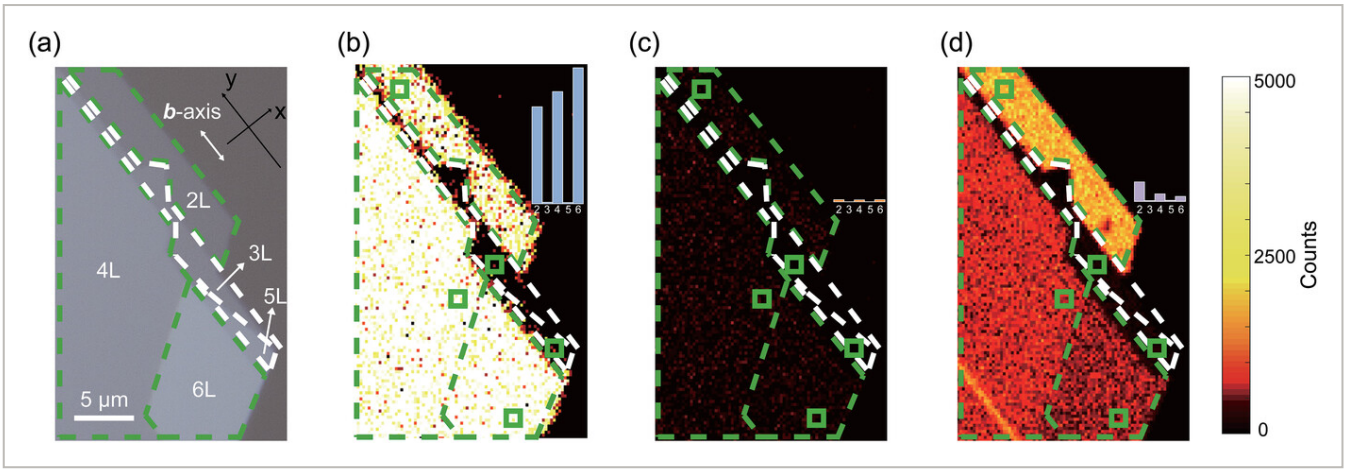

Figure 2

Open in figure viewer | PowerPoint

a) Optical microscopy image of the few-layer ReS_2 sample exfoliated on PDMS. Even-layer areas are marked by green dotted lines, odd-layer areas are marked by white dotted lines. SHG signal microscopy of the same area in (a), upon excitation by photon energies of b) 0.80, c) 0.97, and d) 1.54 eV respectively, with an average power of 0.3 mW. The histogram insets in (b), (c), and (d) indicate the relative SHG intensities extracted at the green rectangles marked in the microscopy regions of different layer numbers.

2.2 Excitation Photon Energy Dependence of SHG

The SHG signals for AB_y-stacked even-layer samples also show strong dependences on the excitation photon energy, as shown in Figure 2b–d. The even-layer regions exhibit observable SHG with approximately uniform signal for samples with the same layer number, and we extract and compare the relative amplitude of the signals from the green rectangle in Figure 2, which are emphasized as the histogram in the top of each diagram. When the fundamental photon energy is 1.54 eV, the SHG intensity for the bilayer is much stronger than that for the six-layer; when the fundamental photon energy changes to 0.97 eV, the SHG intensities for different layer numbers are approximately the same. Furthermore, for all even-layer samples the SHG intensities at an excitation energy of 0.8 eV are much stronger than those at other photon energies. It can be seen that the layer number dependence at 0.8 eV is consistent with the results reported in literature,[13, 14] where the signal intensity increases with layer number; however, such dependence becomes very weak for 0.97 eV, and opposite that for 1.54 eV. These results indicate a strong photon energy dependence for SHG.

To clarify such dependence, we extract the effective bulk susceptibility ($\chi^{(2)}$) spectra for SHG in AB_y-stacked even-layer ReS_2 for the fundamental photon energy varying from 0.74 to 1.55 eV, with fixed linear polarization direction along the 45° direction with respect to the *x*-axis. Such spectra are strongly related to both the band structures and exciton binding energies.[24, 26] Here we measured the total SHG signals in an AB_y-stacked sample. The

magnitude of the effective bulk SHG susceptibility $\chi^{(2)}$ is estimated using an isotropic thin film model (see details in Supporting Information) from the SHG intensities $I_{2\omega}$ collected by the detector and the fundamental light intensity I_0. The thin film model gives

$$\chi^2 = \sqrt{\frac{I_{2\omega}}{I_0^2}} \cdot \sqrt{2c\varepsilon_0} \cdot \frac{\lambda_{2\omega}}{\pi h} \cdot \frac{1}{|\,1 + {R_\omega}^2 \cdot 1 + R_{2\omega}\,|} \quad (1)$$

where ω is the angular frequency of the fundamental laser, h is the thickness of ReS_2 layers, c is the speed of light in vacuum, ε_0 is the dielectric constant of vacuum, and $R_\omega(R_{2\omega})$ gives the reflectivity of the whole structure at $\omega(2\omega)$. For a transparent PDMS substrate, R_ω and $R_{2\omega}$ are close to zero. **Figure** 3a shows the fundamental photon energy dependence of $|\,\chi^{(2)}\,|$ of bilayer, four-layer and six-layer ReS_2. Although the relative SHG intensities do not show a definite layer number dependence for different excitation photon energy, the amplitude of $\chi^{(2)}$ always takes its largest values for the bilayer and its smallest values for the six layer samples. All spectra show two prominent narrow peaks located at photon energies of around 0.8 and 1.5 eV, respectively, and one broad peak located between 1.0 and 1.4 eV. The broad peak is induced by the resonance with electron-hole pairs above the band gap.[27]

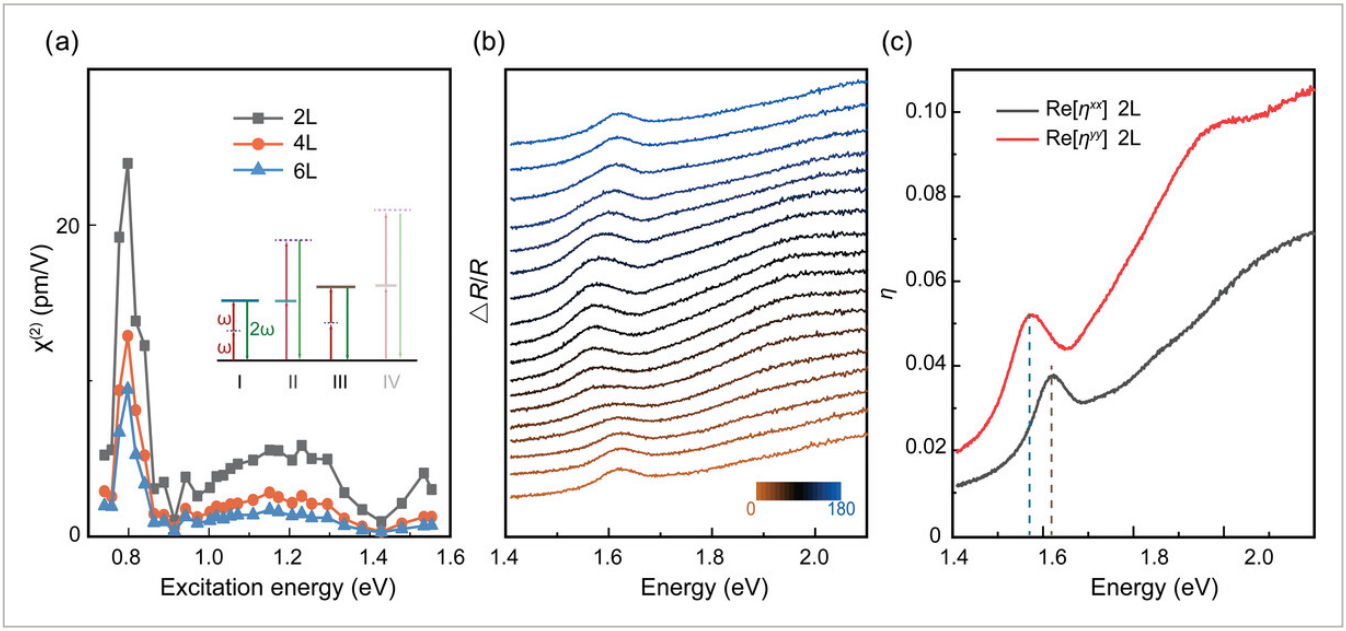

Figure 3

Open in figure viewer | PowerPoint

a) Second-order nonlinear susceptibility ($\chi^{(2)}$) as a function of excitation photon energy. Inset: diagrams for the one- or two-photon resonant transitions to the exciton levels. b) Polarization-resolved reflection spectra of AB_y-stacked bilayer ReS_2 for θ from 0° to 180°. The angle θ is between the incident polarization direction and the *x*-axis. c) The photon energy dependence of the real part of optical conductivity $\mathrm{Re}[\eta^{xx}]$ and $\mathrm{Re}[\eta^{yy}]$ of AB_y-stacked bilayer ReS_2.

Here we give a detailed discussion on the two narrow peaks by taking AB_y-stacked bilayer ReS_2 as an example. Resonant SHG can occur in two optical transition processes by

matching the exciton energy with either the fundamental photon energy (one-photon process) or the SHG photon energy (two-photon process). In general, there might exist different symmetry constraints for one- and two-photon processes. But in AB_y-stacked bilayer ReS_2, these two processes should both be available due to the very low crystal symmetry. Note that due to the existence of two nearly degenerate exciton levels,[4, 10, 28] there are in total four different resonant transitions, as shown in the inset of Figure 3a (I and II, or III and IV).

Theoretical calculations indicate that these two anisotropic excitons have totally different optical responses along the xx (Γ-*M*2) and yy (Γ-*K*1) directions,[10, 28] where the peaks for the real part of optical conductivity components $\mathrm{Re}[\eta^{xx}]$ and $\mathrm{Re}[\eta^{yy}]$ are located at different photon energies. We show that they can be experimentally determined by the polarization-dependent differential reflectance, $\Delta R / R = (R^{'} - R) / R \propto \mathrm{Re}[\eta]$, where $R^{'}(R)$ represents the reflectivity for the whole structure with (without) the ReS_2 sample (see part 3 in Supporting Information). Figure 3b shows the polarization-dependent differential reflectance for AB_y-stacked bilayer sample, and Figure 3c gives the extracted spectra for the real parts of the optical conductivities for a bilayer sample. Two anisotropic exciton energies for the bilayer can be determined by the peak locations at 1.56 and 1.61 eV, marked by two dotted lines. These results are consistent with previous theoretical predictions.[10, 28] For the AB_y-stacked bilayer ReS_2, the peak at ~0.8 eV in the SHG spectra is close to the half of both exciton energies, and it is attributed to a combination of the two-photon resonant processes I and III as shown in Figure 3a. Only one peak appears in the SHG spectra instead of two because of the large broadening of excitonic peaks at room temperature; this is very similar to the differential reflectance spectra as shown in Figure 3b. The peak located at around 1.54 eV, which is very close to the low exciton energy of 1.56 eV, and could be induced by the one-photon process II in Figure 3a. The energy difference of 20 meV may imply the importance of thermal broadening of electronic states, which could be confirmed by experiment at different temperatures,[29] but that is beyond the scope of this work. Our results show that SHG in AB_y-stacked bilayer ReS_2 can be greatly tuned by varying the excitation photon energy, especially around the excitonic resonances.

2.3 Polarization Dependence of SHG

Now we turn to the polarization dependence of SHG at different excitation photon energies. This can be used to identify the relative amplitudes of the different susceptibility components. At normal incidence, there are six non-zero SHG susceptibility tensor components $\chi^{(2)}_{\mathrm{dxx}}$, $\chi^{(2)}_{\mathrm{dyy}}$, $\chi^{(2)}_{\mathrm{dxy}}$, $(d = x,\ y)$, which in general are complex numbers. For incident light $E_{\mathrm{inc}} = E_0 \begin{pmatrix} \cos\theta \\ \sin\theta \end{pmatrix}$, with θ the angle between the polarization of incident light and the *x*-axis. The SHG polarization is $P_{\mathrm{shg}} = E_0^2 \begin{pmatrix} \mathrm{p}_x(\theta) \\ \mathrm{p}_y(\theta) \end{pmatrix}$ with

$$\mathrm{p}_d\theta = \chi^2_{\mathrm{dxx}}\cos^2\theta + \chi^2_{\mathrm{dyy}}\sin^2\theta + \chi^2_{\mathrm{dxy}}\sin 2\theta \quad (2)$$

The experiment collects SHG signals that are polarized along the direction $\begin{pmatrix}\cos\phi\\ \sin\phi\end{pmatrix}$, with ϕ the angle between the polarization of analyzer and the *x*-axis, and the detected SHG field intensity is $I(\theta,\phi) = 2c\varepsilon_0 \mid E_{\text{out}}(\theta,\phi)|^2$ with $E_{\text{out}}(\theta,\phi) \propto E_0^2[\mathrm{p}_x(\theta)\cos\phi + \mathrm{p}_y(\theta)\sin\phi]$.

A widely adopted procedure is to measure two specific patterns: $\mathrm{I}_{\parallel} = I(\theta,\theta)$ (for parallel response (*XX*) and $\mathrm{I}_{\perp} = I(\theta,\theta+\pi/2)$ for perpendicular response (*XY*). **Figure 4a–c** presents the SHG pattern of bilayer ReS_2 excited at the different fundamental photon energies of 0.80, 0.97, and 1.54 eV, respectively. The patterns are totally different than those of other TMD materials,[26, 30] and the largest difference between the parallel and perpendicular responses are shown at angles θ of around 40°, 80°, and 150° for these three photon energies, respectively, indicated by green line in Figure 4a–c. Interestingly, the pattern shape is strongly dependent on the excitation photon energy, that is, different susceptibility components have different photon energy dependences; the values are shown in Table S2, Supporting Information. We attribute this result to the different electronic states accessed at excitation photon energy[18] instead of to any symmetry changes. To fit all susceptibility components, the data of $I(\theta,\phi)$ at different θ and ϕ are used to improve the accuracy, instead of using only $\mathrm{I}_{\parallel}$ and $\mathrm{I}_{\perp}$. For an AB_y-stacked bilayer ReS_2 sample with photon energy 1.55 eV for $\theta \subset (120,300)$, $\phi \subset (50,300)$, the experimental results as well as the fitted curve are shown in Figure 4d, and the fitted values of susceptibility components are listed in Table S3, Supporting Information. Furthermore, the polarization dependence for AB_y-stacked four-layer or six-layer ReS_2 are also measured and show similar properties, as shown in Figure S9, Supporting Information. These values qualitatively confirm the strong anisotropy of few-layer ReS_2, which should be carefully considered in device design for applications.

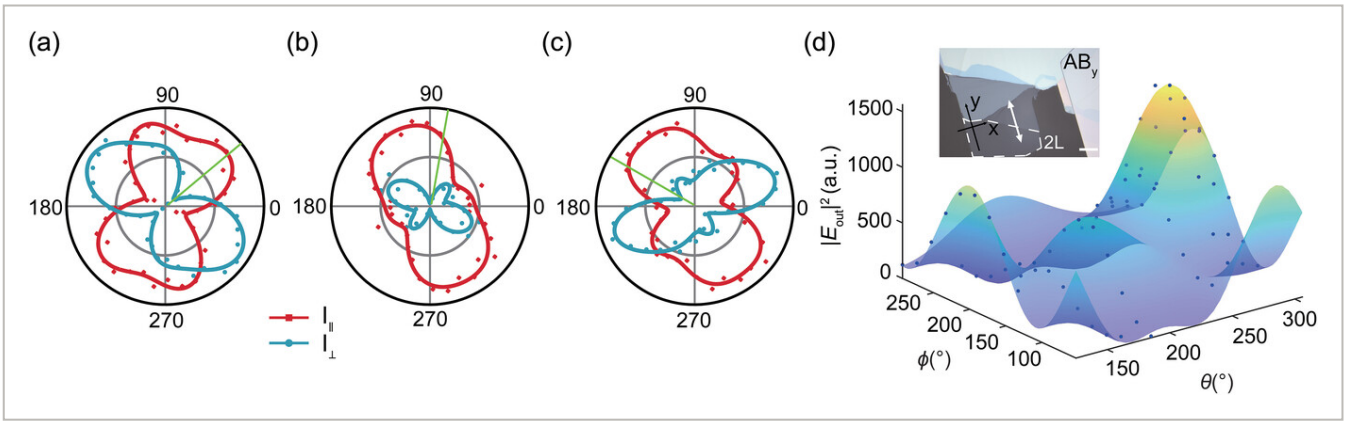

Figure 4

Open in figure viewer | PowerPoint

Polar plot of second harmonic intensities for bilayer ReS_2 (optical microscopy image as shown in Figure 2a) excited by fundamental photon energies of a) 0.80, b) 0.97, and c) 1.54 eV, respectively. The average incident laser power is 0.3 mW. The polar angle is between the laser polarization direction and the *x*-axis. Dots represent experimental data and solid lines are fitted results. The green lines represent the angles for the maximal value of $\mathrm{I}_{\parallel}$ / $\mathrm{I}_{\perp}$. d) Experimental

data of angle-dependent SHG intensities (blue dots) and simulated data (surface diagram) of $|E_{\text{out}}(\theta,\phi)|^2$. Inset: the optical microscope image of the AB_y-stacked bilayer ReS_2 sample with the direction of ***b***-axis indicated by the white arrow. The scale bar is 10 μm.

3 Conclusion

In summary, we have experimentally investigated the SHG in mechanically exfoliated few-layer ReS_2 as well as its dependence on the stacking order, fundamental photon energy, and light polarization. The SHG signals were observed only in $(AB_y)_n$-stacked even-layer samples, where the atomic structure of the B_y layer is a mirror of that of the A layer with mirror planes perpendicular to the ***b***-axis, followed by a one-tenth displacement along this axis; and SHG vanished in all A_n- and $(AB_y)_nA$-stacked samples. The effective bulk susceptibilities for SHG active samples show strong dependence on the excitation photon energy and light polarization. The spectra include resonant peaks when either the fundamental or the second harmonic photon energy matches the two nearly degenerate exciton energies. The individual contribution from each exciton level is physically interesting and important, but it cannot be resolved in our experiments at room temperature due to the large temperature-related broadening; characterization might be possible using low-temperature SHG measurements.[25, 29, 31] Due to the very low crystal symmetry, the light polarization dependence of SHG becomes extremely irregular and photon energy related. Unlike in SHG experiments from other TMD materials, SHG here fails to identify the crystal axis of ReS_2. Our results provide a physical understanding of the SHG in few-layer ReS_2, which will promote the development of the nonlinear photonic devices.

4 Experimental Section

Sample Preparation

The few-layer ReS_2 samples were fabricated on PDMS substrates by mechanical exfoliation of bulk ReS_2 crystals (HQ graphene).

Optical Measurements

Both the photoluminescence (PL) and Raman measurements were performed by using a spectrometer (HORIBA Scientific) with 532 nm laser at normal incidence. The excitation laser was linearly polarized with a power of 54 μW. The polarization-resolved Raman spectroscopy was obtained by rotating the sample to change the angle between the cleaved edge (***b***-axis) and incident laser polarization. All SHG measurements were conducted with a home-built ambient sample-scanning confocal scanning optical microscopy in a back-scattered geometry. A linearly polarized femtosecond laser (Maitai HP and Inspire Auto, Spectra Physics, 151 fs, 80 MHz) with tunable wavelength of 690–1680 nm was used as the fundamental excitation beam, which was focused by an objective (Nikon, 100×, NA = 0.95, or 60×, NA = 0.7) on few-layer ReS_2 at normal incidence. The reflected SHG signal was collected

by the same objective. After passing through a dichroitic beam splitter and two band-pass filters, the SHG signal was collected by either a fiber-coupled spectrometer (Princeton Instruments) or a single-photon counting silicon avalanche photodetector. The SHG microscopy images were obtained by raster scanning the sample on a piezo-actuated 2D nano positioning stage. The typical dwell time at each pixel was ~50 ms. When the azimuthal anisotropy pattern of the SHG was detected, the polarization of the excitation light was rotated using an achromatic half-wave Fresnel rhomb before the microscopic objective. The collected SHG signal was analyzed by a linear polarizer in front of detectors. All measurements were done in atmosphere and at room temperature.

Acknowledgements

This work was supported by the National Natural Science Foundation of China (Grant No. 62121005, Grant No. 12034003), National Natural Science Foundation of China Youth Science Foundation (Grant No. 12004379), and the Key Research Program of Frontier Sciences, CAS (Grant No. ZDBS-LY-JSC026). The authors also thank the Sinoma Institute of Materials Research (Guang Zhou) Co., Ltd. (SIMR) for their assistance with the STEM characterization and Shanghai Ideaoptics Technology Co., Ltd. for their assistance with the angle-resolved reflectance spectra measurements. The authors acknowledge Prof. J. E. Sipe, Shiwei Wu, Tao Jiang, and Di Huang for valuable discussions and proof reading of the manuscript.

Conflict of Interest

The authors declare no conflict of interest.

Author Contributions

Y.W.S. and J.L.C. conceived and supervised the project. Y.S. and Y.W.S. conducted the experimental measurements. Y.S. performed the samples preparation. W.M.W., Z.M.S., and J.L.C. performed the theoretical calculations. Y.S., Y.W.S., and J.L.C. analyzed the data. All of the authors discussed the results and wrote the paper.

Open Research

Data Availability Statement

The data that support the findings of this study are available from the corresponding author upon reasonable request.

Supporting Information

Filename	Description
adom202300111-sup-0001-SuppMat.pdf 1.1 MB	Supporting Information

Please note: The publisher is not responsible for the content or functionality of any supporting information supplied by the authors. Any queries (other than missing content) should be directed to the corresponding author for the article.

References

1 S. Sim, D. Lee, A. V. Trifonov, T. Kim, S. Cha, J. H. Sung, S. Cho, W. Shim, M.-H. Jo, H. Choi, *Nat. Commun.* 2018, **9**, 351.

PubMed | Web of Science® | Google Scholar

2 S. Sim, D. Lee, M. Noh, S. Cha, C. H. Soh, J. H. Sung, M.-H. Jo, H. Choi, *Nat. Commun.* 2016, **7**, 13569.

CAS | PubMed | Web of Science® | Google Scholar

3 S. Tongay, H. Sahin, C. Ko, A. Luce, W. Fan, K. Liu, J. Zhou, Y.-S. Huang, C.-H. Ho, J. Yan, D. F. Ogletree, S. Aloni, J. Ji, S. Li, J. Li, F. M. Peeters, J. Wu, *Nat. Commun.* 2014, **5**, 3252.

CAS | PubMed | Web of Science® | Google Scholar

4 O. B. Aslan, D. A. Chenet, A. M. van der Zande, J. C. Hone, T. F. Heinz, *ACS Photonics* 2016, **3**, 96.

CAS | Web of Science® | Google Scholar

5 Q. Cui, J. He, M. Z. Bellus, M. Mirzokarimov, T. Hofmann, H.-Y. Chiu, M. Antonik, D. He, Y. Wang, H. Zhao, *Small* 2015, **11**, 5565.

CAS | PubMed | Web of Science® | Google Scholar

6 D. A. Chenet, O. B. Aslan, P. Y. Huang, C. Fan, A. M. van der Zande, T. F. Heinz, J. C. Hone, *Nano Lett.* 2015, **15**, 5667.

CAS | PubMed | Web of Science® | Google Scholar

7 A. McCreary, J. R. Simpson, Y. Wang, D. Rhodes, K. Fujisawa, L. Balicas, M. Dubey, V. H. Crespi, M. Terrones, A. R. H. Walker, *Nano Lett.* 2017, **17**, 5897.

CAS | PubMed | Web of Science® | Google Scholar

8 Y.-C. Lin, H.-P. Komsa, C.-H. Yeh, T. Bjorkman, Z.-Y. Liang, C.-H. Ho, Y.-S. Huang, P.-W. Chiu, A. V. Krasheninnikov, K. Suenaga, *ACS Nano* 2015, **9**, 11249.

CAS | PubMed | Web of Science® | Google Scholar

9 Y. Wan, T. Hu, X. Mao, J. Fu, K. Yuan, Y. Song, X. Gan, X. Xu, M. Xue, X. Cheng, C. Huang, J. Yang, L. Dai, H. Zeng, E. Kan, *Phys. Rev. Lett.* 2022, **128**, 067601.

CAS | PubMed | Web of Science® | Google Scholar

10 J. P. Echeverry, I. C. Gerber, *Phys. Rev. B* 2018, **97**, 075123.

CAS | Web of Science® | Google Scholar

11 Q. Cui, R. A. Muniz, J. E. Sipe, H. Zhao, *Phys. Rev. B* 2017, **95**, 165406.

Web of Science® | Google Scholar

12 X. Meng, Y. Zhou, K. Chen, R. H. Roberts, W. Wu, J.-F. Lin, R. T. Chen, X. Xu, Y. Wang, *Adv. Opt. Mater.* 2018, **6**, 1800137.

Web of Science® | Google Scholar

13 Y. Song, S. Hu, M.-L. Lin, X. Gan, P.-H. Tan, J. Zhao, *ACS Photonics* 2018, **5**, 3485.

CAS | Web of Science® | Google Scholar

14 K. P. Dhakal, H. Kim, S. Lee, Y. Kim, J. Lee, J.-H. Ahn, *Light: Sci. Appl.* 2018, **7**, 98.

PubMed | Web of Science® | Google Scholar

15 X. Gan, M. Zhang, Y. Liu, Z.-D. Luo, J. Wang, N. Han, Y. Hao, J. Zhao, X. Chen, *ACS Nano* 2022, **16**, 6404.

PubMed | Web of Science® | Google Scholar

16 Y. Zhou, N. Maity, J.-F. Lin, A. K. Singh, Y. Wang, *ACS Photonics* 2021, **8**, 405.

CAS | Web of Science® | Google Scholar

17 Y. Shan, Y. Li, D. Huang, Q. Tong, W. Yao, W.-T. Liu, S. Wu, *Sci. Adv.* 2018, **4**, eaat0074.

PubMed | Web of Science® | Google Scholar

18 Z. Y. Sun, Y. F. Yi, T. C. Song, G. Clark, B. Huang, Y. W. Shan, S. Wu, D. Huang, C. L. Gao, Z. H. Chen, M. McGuire, T. Cao, D. Xiao, W. T. Liu, W. Yao, X. D. Xu, S. W. Wu, *Nature* 2019, **572**, 497.

CAS | PubMed | Web of Science® | Google Scholar

19 Z. L. Ni, H. Q. Zhang, D. A. Hopper, A. V. Haglund, N. Huang, D. Jariwala, L. C. Bassett, D. G. Mandrus, E. J. Mele, C. L. Kane, L. Wu, *Phys. Rev. Lett.* 2021, **127**, 187201.

CAS | PubMed | Web of Science® | Google Scholar

20 J. J. Dean, H. M. van Driel, *Appl. Phys. Lett.* 2009, **95**, 261910.

Web of Science® | Google Scholar

21 X.-F. Qiao, J.-B. Wu, L. Zhou, J. Qiao, W. Shi, T. Chen, X. Zhang, J. Zhang, W. Ji, P.-H. Tan, *Nanoscale* 2016, **8**, 8324.

CAS | PubMed | Web of Science® | Google Scholar

22 Y. Zhou, N. Maity, A. Rai, R. Juneja, X. Meng, A. Roy, Y. Zhang, X. Xu, J.-F. Lin, S. K. Banerjee, A. K. Singh, Y. Wang, *Adv. Mater.* 2020, **32**, 1908311.

CAS | Web of Science® | Google Scholar

23 R. He, J.-A. Yan, Z. Yin, Z. Ye, G. Ye, J. Cheng, J. Li, C. H. Lui, *Nano Lett.* 2016, **16**, 1404.

CAS | PubMed | Web of Science® | Google Scholar

24 L. M. Malard, T. V. Alencar, A. P. M. Barboza, K. F. Mak, A. M. de Paula, *Phys. Rev. B* 2013, **87**, 201401.

CAS | Web of Science® | Google Scholar

25 K. L. Seyler, J. R. Schaibley, P. Gong, P. Rivera, A. M. Jones, S. Wu, J. Yan, D. G. Mandrus, W. Yao, X. Xu, *Nat. Nanotechnol.* 2015, **10**, 407.

CAS | PubMed | Web of Science® | Google Scholar

26 C. Janisch, Y. Wang, D. Ma, N. Mehta, A. L. Elias, N. Perea-Lopez, M. Terrones, V. Crespi, Z. Liu, *Sci. Rep.* 2014, **4**, 5530.

CAS | PubMed | Web of Science® | Google Scholar

27 M. L. Trolle, G. Seifert, T. G. Pedersen, *Phys. Rev. B* 2014, **89**, 235410.

CAS | Web of Science® | Google Scholar

28 H.-X. Zhong, S. Gao, J.-J. Shi, L. Yang, *Phys. Rev. B* 2015, **92**, 115438.

CAS | Web of Science® | Google Scholar

29 J. Wang, Y. J. Zhou, D. Xiang, S. J. Ng, K. Watanabe, T. Taniguchi, G. Eda, *Adv. Mater.* 2020, **32**, 2001890.

CAS | Web of Science® | Google Scholar

30 N. Kumar, S. Najmaei, Q. Cui, F. Ceballos, P. M. Ajayan, J. Lou, H. Zhao, *Phys. Rev. B* 2013, **87**, 161403(R).

CAS | Web of Science® | Google Scholar

31 G. Wang, X. Marie, I. Gerber, T. Amand, D. Lagarde, L. Bouet, M. Vidal, A. Balocchi, B. Urbaszek, *Phys. Rev. Lett.* 2015, **114**, 097403.

CAS | PubMed | Web of Science® | Google Scholar